IEEE Access
Multidisciplinary | Rapid Review | Open Access Journal

Received August 12, 2019, accepted August 23, 2019, date of publication September 2, 2019, date of current version September 26, 2019.

Digital Object Identifier 10.1109/ACCESS.2019.2938803

Practical Synchronous Steering Angle Control of a Dual-Motor Driving Steer-by-Wire System

HYEONGJIN HWANG[1],*, HYUNGJEEN CHOI[2],*, AND KANGHYUN NAM[1]
[1]School of Mechanical Engineering, Yeungnam University, Gyeongsan 38541, South Korea
[2]Korea Automotive Technology Institute, Cheonan 31214, South Korea

Corresponding author: Kanghyun Nam (khnam@yu.ac.kr)

This work was supported in part by the National Research Foundation of Korea (NRF) grant funded by the Korean Government (MSIT) under Grant 2019R1F1A1061548, and in part by the Yeungnam University Research under Grant 217A580015.

*Hyeongjin Hwang and Hyungjeen Choi are co-first authors.

ABSTRACT Recently, dual-motor driving steer-by-wire (SbW) systems have been introduced and have received considerable attention because they can overcome the limitations of single motor driving SbW systems, which cannot provide large torques required by commercial vehicles and are vulnerable to faults. The two main issues on the performance of the dual-motor driving SbW systems is to ensure steering robustness against model uncertainties, external disturbances, and road condition changes and to synchronize the steering angle. In this paper, a sliding mode controller (SMC) with a disturbance observer (DOB) under master-slave control is proposed to tackle these issues. The combination of an SMC and a DOB is employed to guarantee strong robustness against model uncertainties and external disturbances. In addition, master-slave control is applied to enhance the synchronization performance of dual motor driving SbW systems with significantly different dynamic and response characteristics. Comparative experimental studies are conducted to verify the excellent performance of the proposed control scheme for dual-motor driving SbW systems.

INDEX TERMS Dual-motor driving steer-by-wire system, robust control, sliding mode controller, disturbance observer, synchronization control scheme, independent control, master-slave control.

I. INTRODUCTION

Traditional hydraulic power steering (HPS) systems, which have provided remarkable performance for many years, have been replaced by electric power steering (EPS) systems. EPS systems assist the steering effort of the driver using electric actuators, sensors, and an electronic control unit. EPS systems have many advantages over traditional HPS systems in terms of engine efficiency, space efficiency, and cost [1]. In addition, EPS is a key technology for developing autonomous driving in intelligent vehicle systems because the EPS systems have excellent compatibility with other electronic control systems. EPS systems can be divided into the following three types: column-assist-type EPS (C-EPS) systems, pinion-assist-type EPS (P-EPS) systems, and rack-assist-type EPS (R-EPS) systems. C-EPS systems assist the steering effort using a motor mounted on the steering column. Their advantages are simple construction and low cost, but because the motor is mounted on the steering column, the responsiveness of the power transmitted from the motor to the wheels is slow and the steering feel is relatively poor. P-EPS systems assist the steering effort using a motor mounted on the pinion gear. P-EPS systems provide a better steering feel than C-EPS systems because the motor is closer to the wheels, but P-EPS systems are difficult to install structurally. R-EPS systems provide the best steering feel because the motor that assists the steering effort is located on the steering shaft that connects the wheels. In addition, unlike conventional EPS systems, which use gears, R-EPS systems use a belt drive motor, which reduces noise and improves steering feel because of the elasticity of the rubber belt. However, R-EPS systems have the disadvantage that their unit price is the highest. Despite the cost disadvantage, R-EPS systems are being increasingly adopted to provide drivers with a better steering feel.

Many researchers and engineers in the automotive industry are currently investigating steer-by-wire (SbW) systems, which are known to be examples representing the future development direction of EPS systems [2]–[7]. In SbW systems, the mechanical linkages between the steering wheel

The associate editor coordinating the review of this manuscript and approving it for publication was Jianyong Yao.

This work is licensed under a Creative Commons Attribution 4.0 License. For more information, see http://creativecommons.org/licenses/by/4.0/

and wheels of a vehicle are replaced with electric actuators and sensors. Because the SbW systems have no mechanical linkages, they not only offer design flexibility and a comfortable driving experience but also increases fuel economy by reducing weight. In addition, they offers better functionalities such as active steering capability and generating adjustable steering feel and the driver does not feel unnecessary vibrations from the road surface.

One of the major issues on the steering performance of SbW systems is the steering robustness against parameter variations, external disturbances, and road condition changes. Because the motion of a vehicle changes considerably in response to even a small movement of the wheels, the steering angle control performance requires high accuracy. Recently, many researchers have studied advanced control techniques for controlling SbW systems with the aim to realize the excellent performance of these systems. Sliding mode controller (SMC) has been successfully employed in the SbW systems, and good steering performance has been achieved against parameter variations and external disturbances [8]–[12]. It is well known that, for both linear and nonlinear systems, the SMC is widely used as a robust control method for tracking control and stabilization with bounded uncertainties. In addition, the SMC is a highly effective control technique for R-EPS system, which consists of a belt drive motor system. Belt drive motor systems can generate vibration because of compliance and elasticity introduced by force transmission through the belt and because of nonlinear friction characteristics. High performance of a belt drive motor systems requires that the model uncertainties and external disturbances have to be compensated to achieve accurate vibration-free positioning. Some researchers have already applied the SMC with discontinuous control action to ensure the robustness of a belt drive motor system [13]–[15]. Discontinuous control action can cause chattering and ultimately damage the drive train. Consequently, an SMC with continuous control action is required to reduce chattering [16]. However, it is difficult to implement ideal robust control using the chattering-free SMC. Therefore, a research group [17] has combined a chattering-free SMC with a disturbance observer (DOB) to improve the performance of a closed-loop system. The DOB has been widely used as an effective methodology to overcome model uncertainties and external disturbances [18]–[20]. Following this idea, in the present paper, the combination of an SMC without discontinuous control action and a DOB is proposed and practically applied to SbW system.

However, even if the robustness of SbW systems can be guaranteed, they are still vulnerable to faults. Because a SbW system has no mechanical linkages, faults in electrical signals or components of the system can prevent the system from maintaining its normal function and cause safety problems. Therefore, it is essential to establish a fault-tolerant system that maintains normal steering control of the system and does not affect other systems in the vehicle even if a fault occurs in the SbW system. In addition, commercial vehicles still mainly use HPS systems because single motor driving SbW systems cannot provide a sufficient amount of power and torque required by commercial vehicles. To overcome the limitations of single motor driving SbW systems, dual-motor driving SbW systems have been introduced [21]–[23], which not only ensure reliability and stability with fault-tolerant control systems but also meet the large torque requirement of commercial vehicles.

However, the dual motor driving SbW systems encounter a problem associated with the characteristics of a system that use two motors. One fundamental problem in motion control systems is that dual motors must be controlled in a synchronous manner because lack of synchronization causes an error in the resultant path [23]–[25]. Therefore, a major issue on the steering performance of the dual motor driving SbW systems is synchronization of the steering angle. Synchronization can be achieved by either an independent control scheme or a master-slave control scheme. In an independent control scheme, the synchronizing controller treats the dual motors in a similar manner without favoring one motor over the other. This control scheme uses an identical desired trajectory for the motion. It is a very effective method if the dynamic and response characteristics of each motor system are similar. In a master-slave control scheme, the output of the master system with a slow response characteristic is used as the reference for the slave system with a fast response characteristic. Therefore, if the dynamic and response characteristics are significantly different between the dual motors, as in the case of dual motor driving SbW systems, the master-slave control scheme will be appropriate.

This paper proposes a synchronization control scheme based on an SMC with a DOB under master-slave control for dual motor driving SbW systems consisting of R-EPS system and P-EPS system. An SMC with a DOB was applied to the P-EPS system, and an SMC was applied to the R-EPS system under master-slave control. It is shown that the SMC with the DOB designed in this study is capable of driving the steering angle to closely follow the reference steering angle with strong robustness. In addition, because the dynamic and response characteristics of the dual motor driving SbW system are significantly different, master-slave control is effective in increasing the synchronous steering angle control performance. Experimental results are presented to illustrate the relative performance of the control schemes and their competitive advantages.

This paper is organized as follows. Section II presents a mathematical model of the dual motor driving SbW system used in the control components. In section III, the proposed synchronization control schemes are illustrated. In section IV, the proposed robust control algorithm is presented. Experimental results are presented in Section V, which is followed by the conclusions in Section VI.

II. SYSTEM DESCRIPTION

In this section, a mathematical model of the dual motor driving SbW system is presented. As shown in Fig. 1(a), the system consists of the R-EPS and P-EPS systems. The

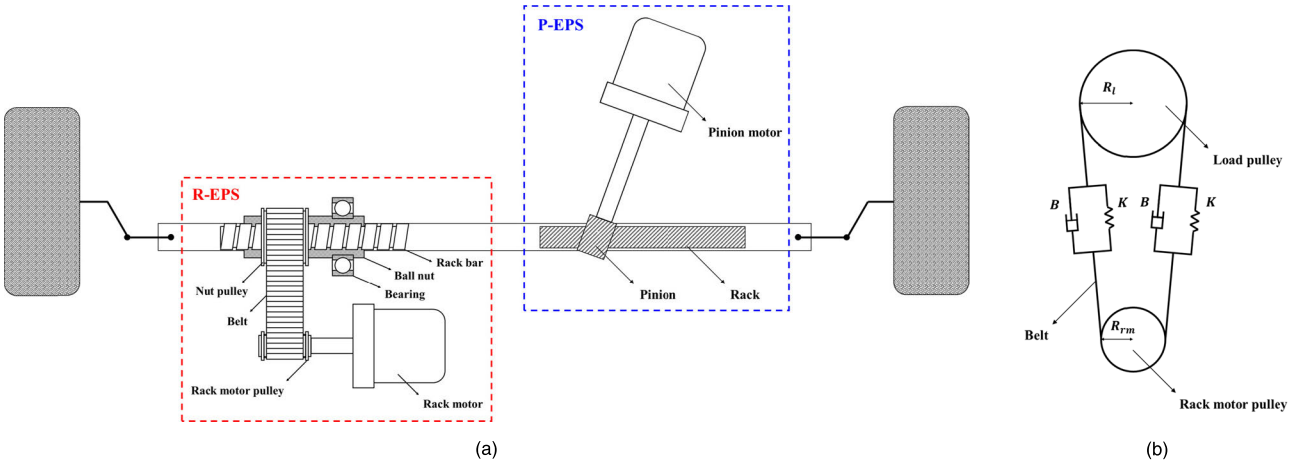

FIGURE 1. Dual-motor driving SbW system model. (a) R-EPS and P-EPS system model. (b) Belt drive motor system model.

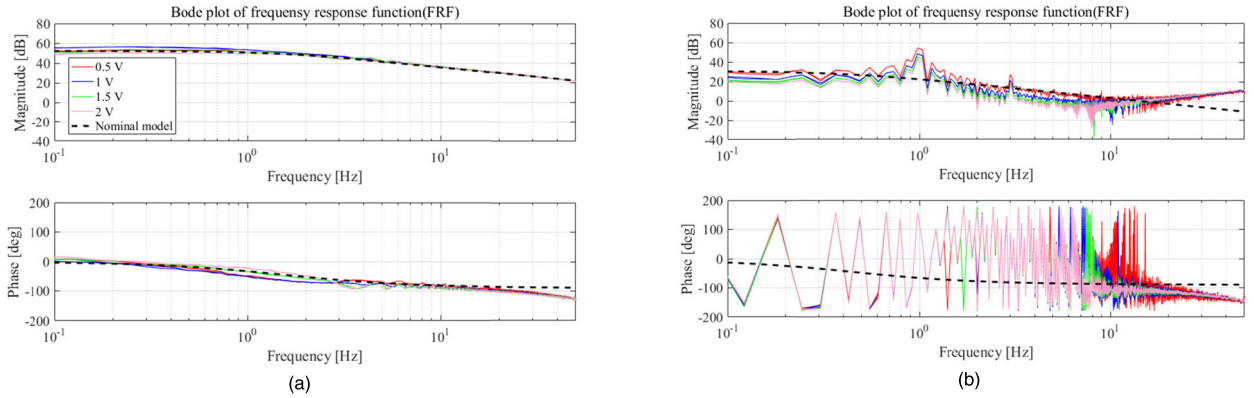

FIGURE 2. Frequency response results. (a) R-EPS system. (b) P-EPS system.

R-EPS system is composed of a rack motor system, which is a belt drive motor system, and a ball screw system. The P-EPS system is composed of a pinion motor system and a rack-and-pinion system.

A. R-EPS

The R-EPS system is shown in Fig. 1(a). The rack motor system, which is a belt drive motor system, as depicted by Fig. 1(b), consists of a belt and two pulleys. The mechanical dynamics model of the R-EPS system is represented as follows:

$$J_{rm}\ddot{\theta}_{rm}(t) + B_{rm}\dot{\theta}_{rm}(t) + 2KR_{rm}\{R_{rm}\theta_{rm}(t) - R_l\theta_l(t)\} + 2BR_{rm}\left\{R_{rm}\dot{\theta}_{rm}(t) - R_l\dot{\theta}_l(t)\right\} = \tau_{rm}(t) - \tau_{frm}\left(\theta, \dot{\theta}\right) \quad (1)$$

$$J_l\ddot{\theta}_l(t) + B_l\dot{\theta}_l(t) + 2KR_l\{R_l\theta_l(t) - R_{rm}\theta_{rm}(t)\} + 2BR_l\left\{R_l\dot{\theta}_l(t) - R_{rm}\dot{\theta}_{rm}(t)\right\} = -\tau_{fl}\left(\theta, \dot{\theta}\right) - \tau_{fbs}\left(\theta, \dot{\theta}\right) \quad (2)$$

where J_{rm} is the moment of inertia of the rack motor, B_{rm} is the viscous friction coefficient of the rack motor, J_l is the moment of inertia of the load, B_l is the viscous friction coefficient of the load, $\ddot{\theta}_{rm}(t)$ is the angular acceleration of the rack motor, $\ddot{\theta}_l(t)$ is the angular acceleration of the load, $\dot{\theta}_{rm}(t)$ is the angular velocity of the rack motor, $\dot{\theta}_l(t)$ is the angular velocity of the load, $\theta_{rm}(t)$ is the angular position of the rack motor, $\theta_l(t)$ is the angular position of the load, K is the elasticity coefficient of the belt, B is the viscous friction coefficient of the belt, R_{rm} is the radius of the rack motor pulley, R_l is the radius of the load pulley, $\tau_{rm}(t)$ is the rack motor driving torque, $\tau_{frm}(\theta, \dot{\theta})$ is the friction torque affecting the rack motor pulley, $\tau_{fl}(\theta, \dot{\theta})$ is the friction torque which affecting the load pulley, $\tau_{fbs}(\theta, \dot{\theta})$ is the friction torque which affecting the ball screw. As shown in (1) and (2), the R-EPS system is a highly coupled and nonlinear system with exogenous disturbances.

To design a model based controller, the nominal model is obtained by measuring the frequency response. In the experiment, chirp signal torque commands, which have a wide frequency range (0.1Hz to 50Hz), are applied to the driving motor. As shown in Fig. 2(a), the frequency response result from the rack motor driving torque to the angular velocity of the rack motor indicates that the mechanical dynamics model can be represented by a first-order system instead of

a higher order system. A transfer function is obtained as follows:

$$\frac{\dot{\theta}_{rm}(t)}{\tau_{rm}(t)} = \frac{1}{J_{nrm}s + B_{nrm}} \tag{3}$$

where J_{nrm} is the nominal moment of inertia of the rack motor and B_{nrm} is the nominal viscous friction coefficient of the rack motor. For position controller design, position nominal model is obtained as follows:

$$P_{nrm}(s) = \frac{\theta_{rm}(t)}{\tau_{rm}(t)} = \frac{1}{J_{nrm}s^2 + B_{nrm}s} \tag{4}$$

From the experimental result, (1) and (2) can be simplified as follows:

$$J_{rm}\ddot{\theta}_{rm}(t) + B_{rm}\dot{\theta}_{rm}(t) = \tau_{rm}(t) - \tau_{frm}\left(\theta, \dot{\theta}\right) - \tau_{fl}\left(\theta, \dot{\theta}\right) - \tau_{fbs}\left(\theta, \dot{\theta}\right) \tag{5}$$

Using a nominal model, (5) can be expressed as follows:

$$J_{nrm}\ddot{\theta}_{rm}(t) + B_{nrm}\dot{\theta}_{rm}(t) = \tau_{rm}(t) + d_{rm}(t) \tag{6}$$

where $d_{rm}(t)$ is the lumped disturbance of the rack motor system which includes external disturbances $\tau_{exrm}\left(\theta, \dot{\theta}\right)$ and model uncertainties. It is represented as follows:

$$\tau_{exrm}\left(\theta, \dot{\theta}\right) = \tau_{frm}\left(\theta, \dot{\theta}\right) + \tau_{fl}\left(\theta, \dot{\theta}\right) + \tau_{fbs}\left(\theta, \dot{\theta}\right) \tag{7}$$

$$d_{rm}(t) = -\Delta J_{rm}\ddot{\theta}_{rm}(t) - \Delta B_{rm}\dot{\theta}_{rm}(t) - \tau_{exrm}\left(\theta, \dot{\theta}\right) \tag{8}$$

where $-\Delta J_{rm} = J_{rm} - J_{nrm}$ and $-\Delta B_{rm} = B_{rm} - B_{nrm}$ are the parametric errors of the mass and viscous friction coefficient.

B. P-EPS

The P-EPS system is depicted in Fig. 1(a). The mechanical dynamics model of the P-EPS system is described as follows:

$$J_{pm}\ddot{\theta}_{pm}(t) + B_{pm}\dot{\theta}_{pm}(t) = \tau_{pm}(t) - \tau_{fpm}\left(\theta, \dot{\theta}\right) \tag{9}$$

where J_{pm} is the moment of inertia of the pinion motor, B_{pm} is the viscous friction coefficient of the pinion motor, $\ddot{\theta}_{pm}(t)$ is the angular acceleration of the pinion motor, $\dot{\theta}_{pm}(t)$ is the angular velocity of the pinion motor, $\tau_{pm}(t)$ is the pinion motor driving torque, and $\tau_{fpm}\left(\theta, \dot{\theta}\right)$ is the friction torque affecting the rack and pinion.

The frequency response characteristics of the P-EPS system were obtained through the same chirp signal torque commands described in section II.A. A transfer function is derived from Fig. 3 is as follows:

$$\frac{\dot{\theta}_{pm}(t)}{\tau_{pm}(t)} = \frac{1}{J_{npm}s + B_{npm}} \tag{10}$$

$$P_{npm}(s) = \frac{\theta_{pm}(t)}{\tau_{pm}(t)} = \frac{1}{J_{npm}s^2 + B_{npm}s} \tag{11}$$

Using a nominal model, (9) can be expressed as follows:

$$J_{npm}\ddot{\theta}_{pm}(t) + B_{npm}\dot{\theta}_{pm}(t) = \tau_{pm}(t) + d_{pm}(t) \tag{12}$$

where $d_{pm}(t)$ is the lumped disturbance of the pinion motor system, which includes external disturbances $\tau_{expm}\left(\theta, \dot{\theta}\right)$ and model uncertainties. It is represented as follows:

$$\tau_{expm}\left(\theta, \dot{\theta}\right) = \tau_{fpm}\left(\theta, \dot{\theta}\right) \tag{13}$$

$$d_{pm}(t) = -\Delta J_{pm}\ddot{\theta}_{pm}(t) - \Delta B_{pm}\dot{\theta}_{pm}(t) - \tau_{expm}\left(\theta, \dot{\theta}\right) \tag{14}$$

where $-\Delta J_{pm} = J_{pm} - J_{npm}$ and $-\Delta B_{pm} = B_{pm} - B_{npm}$ are the parametric errors of the mass and viscous friction coefficient.

III. SYNCHRONIZATION CONTROL SCHEMES FOR DUAL-MOTOR DRIVING STEER-BY-WIRE SYSTEM

The synchronization control schemes for the dual motor driving SbW system are illustrated in this section. The schemes are divided into two main classes, as shown in Fig. 3. In the figure, θ_d is the desired angular position of the motor, θ_{m1} is the angular position of motor 1, and θ_{m2} is the angular position of motor 2. The first scheme is an independent control scheme in which an identical desired reference θ_d is given to each motor system in synchronization. The second scheme is a master-slave control scheme in which the output θ_{m1} of the master system serves as a reference for the slave system.

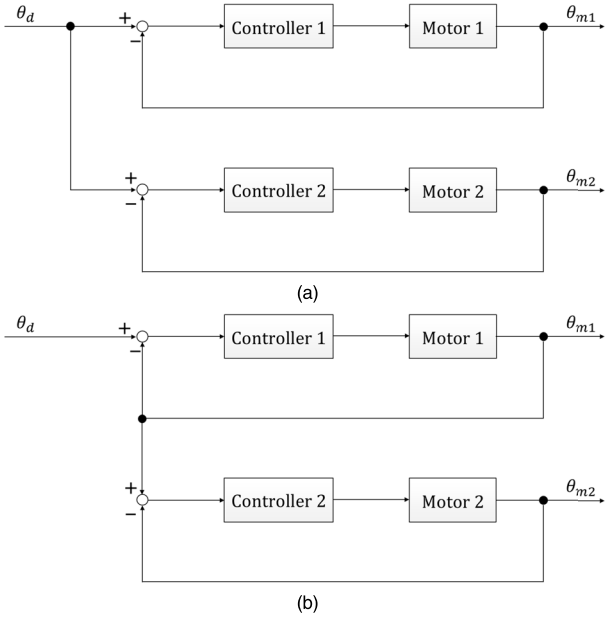

FIGURE 3. Synchronization control schemes. (a) Independent control scheme. (b) Master-slave control scheme.

A. INDEPENDENT CONTROL

In the independent control scheme, the dynamic and response characteristics for each motor system are matched and the references for each motor system are applied in synchronization. The structure of the scheme is shown in Fig. 3(a).

The scheme is very effective if the dynamic and response characteristics of each servo system are similar. In addition,

because the deficiencies of one motor do not directly affect the other motor, this control scheme is superior to a master-slave control scheme in terms of stability. Therefore, even if one of the dual motors fails, this control method that can provide fault-tolerance, thereby allowing the system to continue to operate properly.

However, the main problem with this control scheme is that it is difficult to match the control characteristic of each motor system perfectly. Moreover, it is impossible to synchronize the positions of each system precisely. Therefore, if the dynamic and response characteristics are significantly different between the dual motors, the independent control method may not be the best because the synchronization speed of the overall system is set by the slowest axis. The larger the difference between the response characteristics of the dual motors, the larger is the synchronization error, which is the position difference between the two motors.

B. MASTER-SLAVE CONTROL

In the master-slave control scheme, one motor with a relatively slow response characteristic is chosen as the master motor and the other motor with a relatively fast response characteristic is chosen as the slave motor. The output of the master motor serves as the reference for the slave motor. Fig. 3(b) depicts the structure of the master-slave control scheme.

The merit of this control scheme is that it provides direct compensation for the synchronization error because the slave error is the synchronization error. Therefore, unlike in the case of the independent control scheme, the synchronization error can be reduced even if the dynamic and response characteristics are significantly different among the dual motors.

However, the tracking performance can be actually limited because the actual trajectory of the master motor acts as the commanded trajectory of the slave motor. Compared to a mathematically generated trajectory, a signal-generated trajectory measured from a sensor generates quantization noise, measurement noise, and delay. This causes the actual trajectory of the slave motor to deviate farther from the desired trajectory and makes it difficult to use the feedforward control properly. In addition, when the master motor encounters a disturbance, the slave motor will be able to respond but when the slave motor encounters a disturbance, the master motor will not be able to know the disturbance and address it appropriately.

IV. DESIGN OF ROBUST CONTROL

In this section, the proposed robust control scheme is illustrated. The steering angle control performance of SbW systems requires robustness against model uncertainties and external disturbances. This study employs a combination of an SMC and a DOB to guarantee strong robustness of the system. Because discontinuous control action of an SMC can cause chattering, which increases vibration, an SMC without discontinuous control action was used. The DOB improves the robustness of the SMC without discontinuous

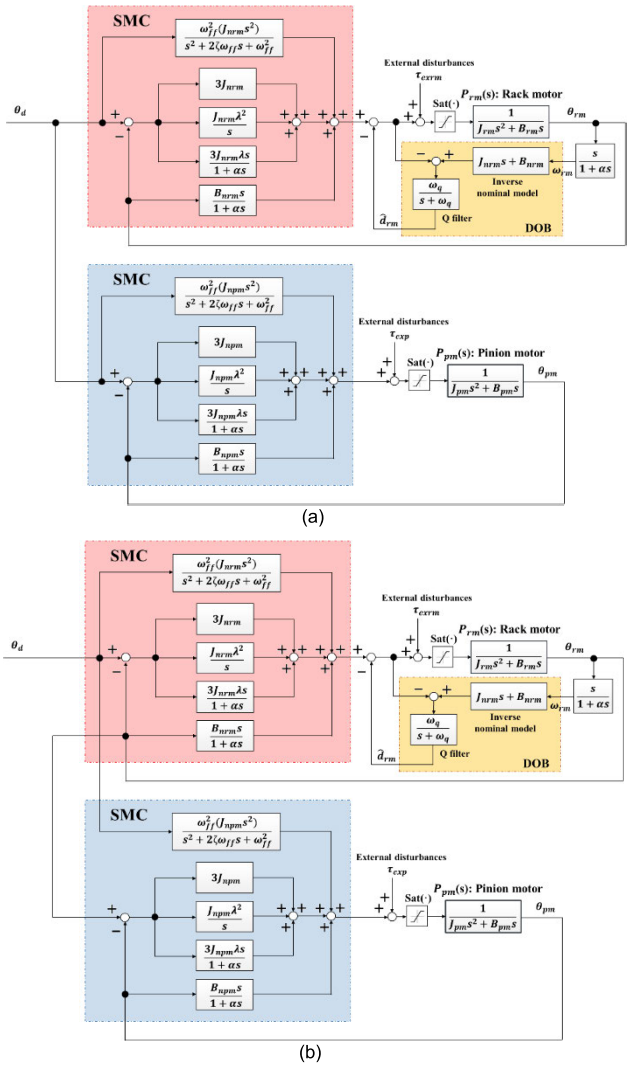

FIGURE 4. Overall block diagram of proposed control schemes for dual motor driving SbW system. (a) Proposed control scheme under independent control. (b) Proposed control scheme under master-slave control.

control action. An overview of the control algorithm is shown in Fig. 4 (a).

A. SLIDING MODE CONTROLLER

The SMC is well known as a robust control method to stabilize nonlinear and uncertain system characteristics. Its features keep systems insensitive to the uncertainties and disturbances on the sliding surface. The conventional SMC design approach consists of two steps. First, a sliding surface is designed so that the system trajectory along the surface performs the desired behavior. Then, a reaching condition is designed so that the system trajectories reach the sliding surface. To achieve the control objective, the tracking error $\varepsilon(t)$ and sliding surface $S(t)$ are defined as follows:

$$\varepsilon(t) = \theta_d(t) - \theta_m(t) \tag{15}$$

$$S(t) = \dot{\varepsilon}(t) + 2\lambda\varepsilon(t) + \lambda^2 \int \varepsilon(t) \tag{16}$$

where $\theta_d(t)$ is the desired angular position of the motor, $\theta_m(t)$ is the angular position of the motor, and λ is the positive feedback gain. To achieve the control requirements, the sliding surface should satisfy the reaching condition as follows:

$$\dot{S}(t) = -\lambda S(t) \tag{17}$$

The dynamic equation of the mechanical model is represented as follows:

$$J_{nm}\ddot{\theta}_m(t) + B_{nm}\dot{\theta}_m(t) = \tau_m(t) + d_m(t) \tag{18}$$

$$\ddot{\theta}_m(t) = \frac{1}{J_{nm}} - B_{nm}\dot{\theta}_m(t) + \tau_m(t) + d_m(t) \tag{19}$$

where J_{nm} is the nominal moment of inertia of the motor, B_{nm} is the nominal viscous friction coefficient of the motor, $\ddot{\theta}_m(t)$ is the angular acceleration of the motor, $\dot{\theta}_m(t)$ is the angular velocity of the motor, $\tau_m(t)$ is the motor driving torque, and $d_m(t)$ is the lumped disturbance of the motor system. From (16), (17), and (19), the following control law $\tau_m(t)$ can be obtained as follows:

$$\tau_m(t) = J_{nm}\ddot{\theta}_d(t) + B_{nm}\dot{\theta}_m(t) + J_{nm} \times \left\{3\lambda\dot{\varepsilon}(t) + 3\lambda^2\varepsilon(t) + \lambda^3\int\varepsilon(t)\right\} - \hat{d}_m(t) \tag{20}$$

where $\hat{d}_m(t)$ is the estimated lumped disturbance of the motor system.

To prove the stability of the proposed control system, Lyapunov theory is used. The positive definite Lyapunov function is as follows:

$$V(t) = \frac{1}{2}S(t)^2, \quad V(t) > 0 \tag{21}$$

The time derivative of (21) is expressed as follows:

$$\begin{aligned}\dot{V}(t) &= S(t)\dot{S}(t)\\ &= S(t)\{-\lambda S(t)\}\\ &= -\lambda S(t)^2 < 0\end{aligned} \tag{22}$$

(21) and (22) clearly show that the tracking error $S(t)$ asymptotically converges to zero and the proposed control system is stable.

B. SLIDING MODE CONTROLLER WITH DISTURBANCE OBSERVER

Using a low pass filter called a Q filter and the inverse of a nominal plant, the DOB estimated the disturbance and the estimated disturbance is used as a disturbance cancellation input. Therefore, the DOB makes the complicated dynamics of the actual system behave as a defined nominal model. The SMC structure with DOB is depicted in Fig. 4 (a). The output of the plant $\theta_m(t)$ is represented by

$$\theta_m(t) = P_{nm}(s)\tau_m(t) - P_{nm}(s)\{1 - Q(s)\}d_m(t) - Q(s)n(t) \tag{23}$$

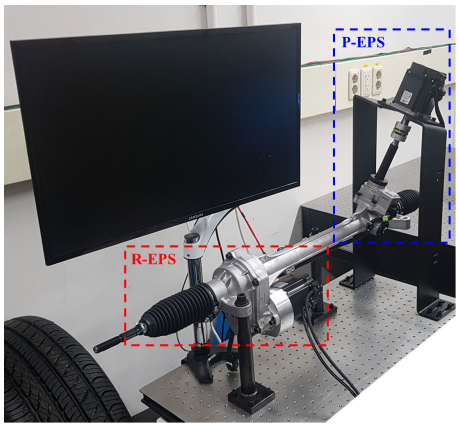

FIGURE 5. Experimental setup for dual motor driving SbW system.

where $P_{nm}(s) = 1/(J_{nm}s^2 + B_{nm}s)$, $Q(s)$ is the Q filter, and $n(t)$ is the noise of the sensor.

In (23), all the transfer functions are stable and the cutoff frequency of the Q filter $Q(s)$ is set to ω_c. If the input frequency is lower than cutoff frequency (i.e., $Q(j\omega) \approx 1, \omega < \omega_c$), the output $\theta(j\omega)$ becomes similar to $\theta(t) = P_{nm}(s)\tau_m(t) - n(t)$. Assuming that the sensor noise mostly exists in the high frequency range (i.e.,$n(j\omega) \approx 0, \omega < \omega_c$), the output $\theta(j\omega)$ is represented by

$$\theta(j\omega) = P_{nm}(j\omega)\tau_m(j\omega) \tag{24}$$

This shows that the actual plant behaves as the nominal model because the lumped disturbance is attenuated by the DOB. Therefore, the model-based controller can be designed by the nominal model.

To prove the stability of the closed-loop control system, the mechanical dynamics model of the motor system using the nominal model is expressed as follows:

$$J_{nm}\ddot{\theta}_m(t) = -B_{nm}\dot{\theta}_m(t) + \tau_m(t) + d_{lm}(t) + d_{hm}(t) \tag{25}$$

where $d_{lm}(t)$ and $d_{hm}(t)$ are the low and high frequency components of the lumped disturbance. From (20) and (23)-(25), the closed-loop error dynamics are obtained as follows:

$$J_{nm}\dddot{\varepsilon}(t) + 3\lambda J_{nm}\ddot{\varepsilon}(t) + 3\lambda^2 J_{nm}\dot{\varepsilon}(t) + \lambda^3 J_{nm}\int\varepsilon(t) = -\dot{\tilde{d}}_{lm}(t) - \dot{d}_{hm}(t) \tag{26}$$

where $-\tilde{d}_{lm}(t) = d_{lm}(t) - \hat{d}_m(t)$ is the estimation error of the low frequency components of the lumped disturbance. Assume that

$$\left\|-\tilde{d}_{lm}(t) - d_{hm}(t)\right\|_\infty < \varepsilon, \quad for\ \exists\varepsilon > 0 \tag{27}$$

In the frequency range below the cutoff frequency of the Q filter $Q(s)$, the closed-loop transfer function from the disturbances to the tracking error is obtained as follows:

$$\frac{\varepsilon(s)}{-\tilde{d}_{lm}(s) - d_{hm}(s)} = \frac{s}{J_{nm}s^3 + 3\lambda J_{nm}s^2 + 3\lambda^2 J_{nm}s + \lambda^3 J_{nm}} \tag{28}$$

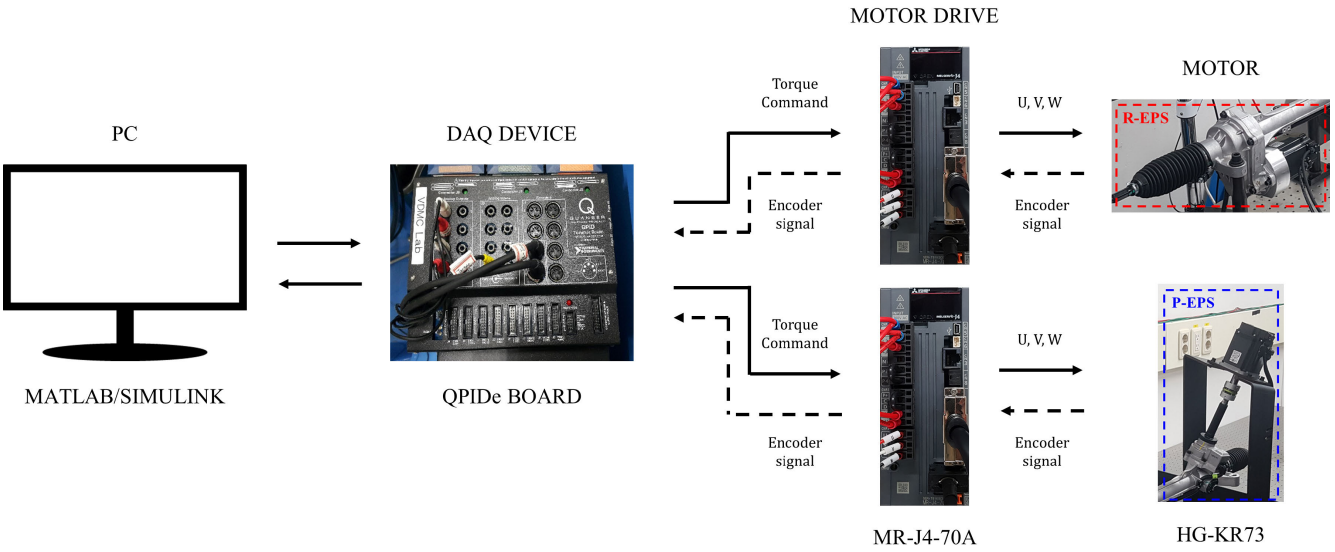

FIGURE 6. Overall control system.

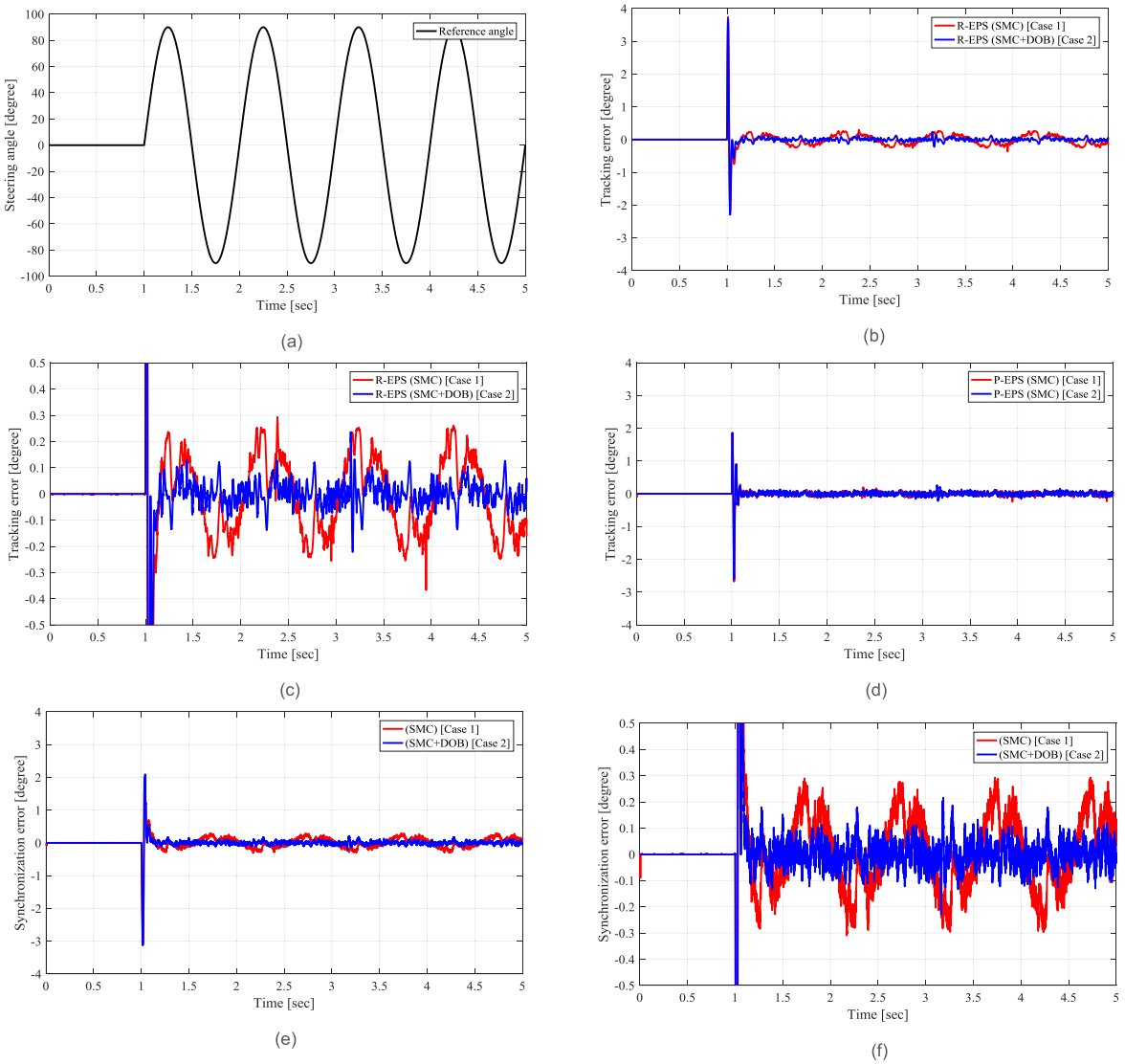

FIGURE 7. Experimental results to verify effectiveness of disturbance observer (sinusoidal position trajectory). (a) Reference angle. (b) Tracking errors of R-EPS. (c) Enlarged figure of (b). (d) Tracking errors of P-EPS. (e) Synchronization errors. (f) Enlarged figure of (e).

TABLE 1. Performance comparisons of controllers (sinusoidal position trajectory).

		Tracking error (degree)		Synchronization error (degree)	
		RMS	MAX	RMS	MAX
Case 1	R-EPS	0.247	3.741	0.231	2.030
	C-EPS	0.144	1.862		
Case 2	R-EPS	0.213	3.678	0.197	2.094
	C-EPS	0.146	1.862		
Case 3	R-EPS	0.214	3.745	0.032	0.156
	C-EPS	0.218	3.785		

TABLE 2. Performance comparisons of controllers (trapezoidal position trajectory).

		Tracking error (degree)		Synchronization error (degree)	
		RMS	MAX	RMS	MAX
Case 1	R-EPS	0.494	3.180	0.431	4.639
	C-EPS	0.313	2.349		
Case 2	R-EPS	0.392	2.935	0.285	3.065
	C-EPS	0.311	2.439		
Case 3	R-EPS	0.391	2.952	0.121	1.002
	C-EPS	0.378	2.799		

In (28), because all the desired poles are designed to be located on the left-half plane, the proposed control system can be stable.

V. EXPERIMENT

In this section, we introduce the dual-motor driving SbW system used in the experiment and the experimental results of the proposed control scheme. To validate the performance of the proposed control scheme, experiments were performed on the overall control system shown in Fig. 6.

A. EXPERIMENTAL SETUP

The dual motor driving SbW system for the experiment is illustrated in Fig. 5 and the overall control system is illustrated in Fig. 6. Two ac motors (Mitsubishi HG-KR73) driven by servo drivers (Mitsubishi MR-J4-70A) were used as the rack motor and pinion motor, respectively. An encoder was installed on each ac motor to measure the angular position of each motor. QPIDe Hardware-in-the-Loop control board of Quanser company was used as a DAQ device for real-time control with a 1-ms sampling time. The proposed control algorithm was implemented on a desktop computer using the QUARC software in MATLAB/SIMULINK.

B. EXPERIMENTAL RESULTS

To verify the performance of the proposed control scheme, we compared three cases. In the first case, the SMC was applied to both R-EPS and P-EPS under independent control. In the second case, the SMC with the DOB was applied to R-EPS and the SMC was applied to P-EPS under independent control. In the third case, the SMC with the DOB was applied to P-EPS and the SMC was applied to R-EPS under master-slave control. The reference angle was given by a sinusoidal position trajectory with a magnitude of 90 degree and a frequency of 1Hz and by a trapezoidal position trajectory, where a maximum position was set to 100 degree and the velocity was 500 degree/s. The experimental results are

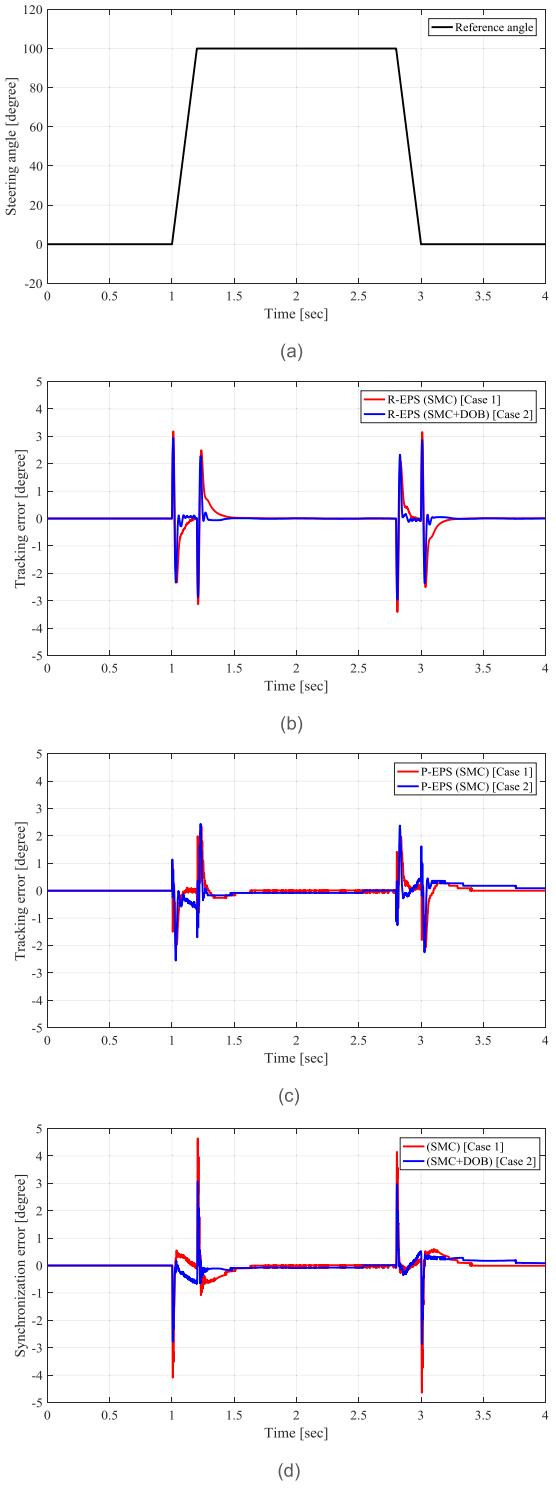

FIGURE 8. Experimental results to verify effectiveness of disturbance obs erver (trapezoidal position trajectory). (a) Referen ce angle. (b) Tracking errors of R-EPS. (c) Tracking errors of P-EPS. (d) Synchronization errors.

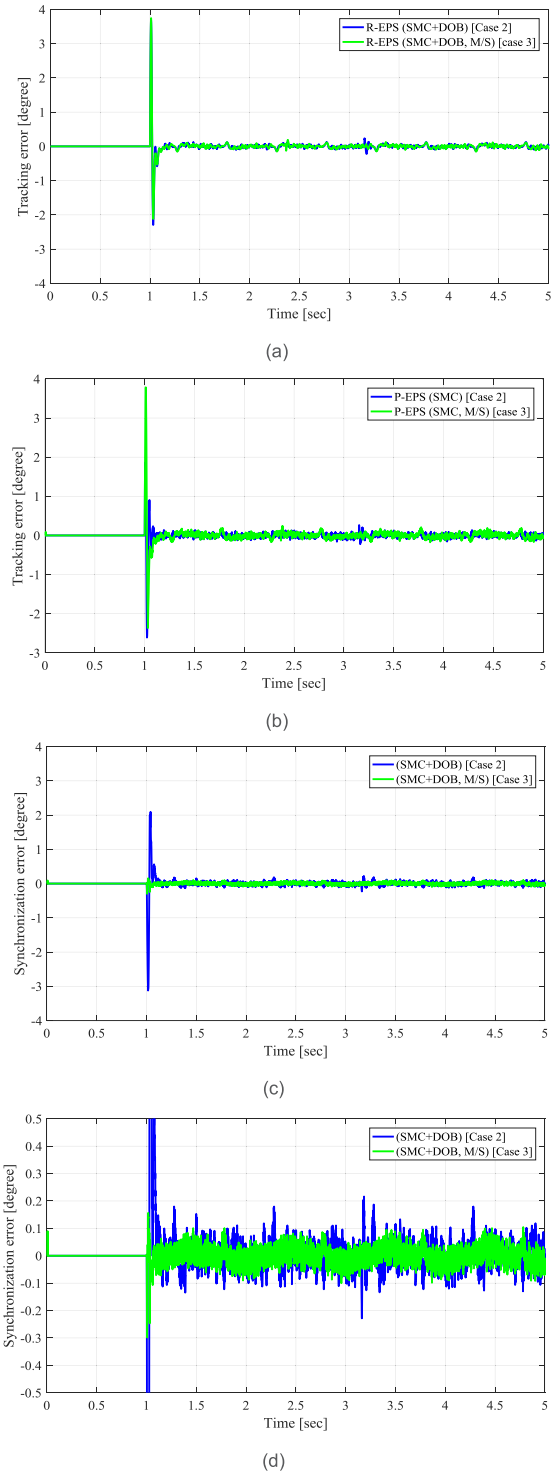

FIGURE 9. Experimental results to verify effectiveness of master-slave contr ol (sinusoidal position trajectory). (a) Tracking errors of R-EPS. (b) Tracking errors of P-EPS. (c) Synchronization errors. (d) Enlarged figure of (c).

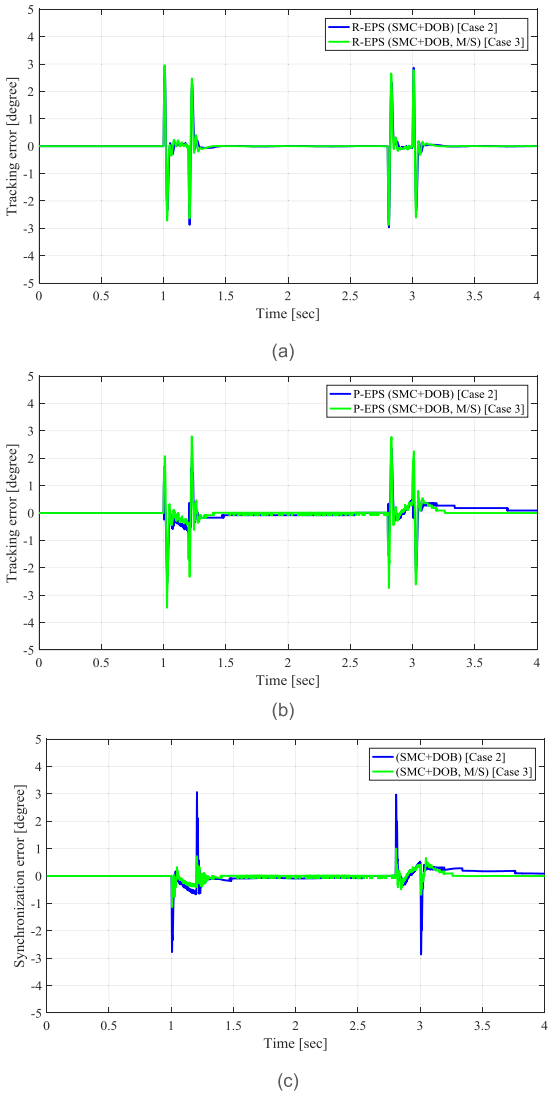

FIGURE 10. Experimental results to verify effectiveness of disturbance observ er (trapezoidal position trajectory). (a) Tracking errors of R-EPS. (b) Tracking errors of P-EPS. (c) Synchronization errors.

shown in Fig. 7-10. The RMS and maximum values of the tracking error and synchronization error are summarized in Table 1 and Table 2.

First, the DOB performance for R-EPS is shown based on a comparison between case 1 and case 2. Fig. 7(b), 7(c), and 8(b) show that the tracking error for R-EPS was reduced when the DOB was applied. As shown in Tables 1 and Table 2, when the DOB was applied, the RMS tracking error value for R-EPS was reduced by 13.7 % for the sinusoidal position trajectory and by 20.6 % for the trapezoidal position trajectory. The maximum tracking error value for R-EPS was reduced by 1.6 % for the sinusoidal position trajectory and by 7.7 % for the trapezoidal position trajectory. These experimental results show that the DOB achieved robustness against model uncertainties and external disturbances. As the tracking error of R-EPS was reduced, the synchronization error was also reduced. Because P-EPS achieved sufficient steering angle control performance with the pure SMC algorithm, only the SMC algorithm was applied to P-EPS. Therefore, the tracking error results for P-EPS were similar in case 1 and case 2.

Second, the experimental results of case 2 were compared with those of case 3 to validate the performance of master-slave control. The tracking error results for R-EPS were

similar because the same algorithm was used. Table 1 and Table 2 show that the RMS and maximum values of the tracking error for P-EPS under master-slave control are larger than the those for P-EPS under independent control because of the noise and delay generated by the signal generation trajectory, which is the reference for the slave system. Fig. 9(c), 9(d), and 10(d) show that the synchronization error was the smallest under master-slave control. As shown in Tables 1 and Table 2, when master-slave control was applied, the RMS synchronization error value was reduced by 83.7 % for the sinusoidal position trajectory and by 57.5 % for the trapezoidal position trajectory. The maximum synchronization error value was reduced by 92.5 % for the sinusoidal position trajectory and by 67.3 % for the trapezoidal position trajectory. These results show that the best synchronous steering angle control performance was achieved when the SMC with the DOB was used under master-slave control.

VI. CONCLUSION

In this paper, the mathematical modeling of dual-motor driving SbW systems has been explored and a novel synchronous control scheme based on an SMC with a DOB under master-slave control has been proposed. The study results indicate that the proposed SMC with the DOB can efficiently alleviate the effects of model uncertainties and external disturbances. In addition, the proposed master-slave control can reduce synchronization errors. Based on experimental results, the excellent steering robustness and synchronous steering angle control performance of the proposed scheme have been verified.

ACKNOWLEDGMENT

(Hyeongjin Hwang and Hyungjeen Choi are co-first authors.)

REFERENCES

[1] A. Badawy, J. Zuraski, F. Bolourchi, and A. Chandy, "Modeling and analysis of an electric power steering system," Steering Suspension Technol. Symp., Detroit, MI, USA, SAE Tech. Paper Series, 1999-01-0399, Mar. 1999.

[2] D. Peter and R. Gerhard, "Electric power steering-the first step on the way to steer by wire," Warrendale, PA, USA, SAE Tech. Paper 1999-01-0401, 1999.

[3] S. Amberkar, F. Bolourchi, J. Demerly, and S. Millsap, "A control system methodology for steer by wire systems," Soc. Automotive Eng. World Congr., Detroit, MI, USA, SAE Tech. Paper 2004-01-1106, 2004.

[4] S.-W. Oh, H.-C. Chae, S.-C. Yun, and C.-S. Han, "The design of a controller for the steer-by-wire system," *JSME Int. J. Ser. C, Mech. Syst. Mach. Elements Manuf.*, vol. 47, no. 3, pp. 896–907, Sep. 2004.

[5] M. Bertoluzzo, G. Buja, and R. Menis, "Control schemes for steer-by-wire systems," *IEEE Ind. Electron. Mag.*, vol. 1, no. 1, pp. 20–27, May 2007.

[6] N. Bajçinca, R. Cortesão, and M. Hauschild, "Robust control for steer-by-wire vehicles," *Auton. Robots*, vol. 19, pp. 193–214, Sep. 2005.

[7] P. Yih and J. C. Gerdes, "Modification of vehicle handling characteristics via steer-by-wire," *IEEE Trans. Control Syst. Technol.*, vol. 13, no. 6, pp. 965–976, Nov. 2005.

[8] H. Wang, H. Kong, Z. Man, D. M. Tuan, Z. Cao, and W. Shen, "Sliding mode control for steer-by-wire systems with AC motors in road vehicles," *IEEE Trans. Ind. Electron.*, vol. 61, no. 3, pp. 1596–1611, Mar. 2014.

[9] F. Zou, D. Song, Q. Li, and B. Yuan, "A new intelligent technology of steering-by-wire system by variable structure control with sliding mode," in *Proc. Int. Joint Conf. Artif. Intell.*, Apr. 2009, pp. 857–860.

[10] M. T. Do, Z. Man, C. Zhang, H. Wang, and F. S. Tay, "Robust sliding mode-based learning control for steer-by-wire systems in modern vehicles," *IEEE Trans. Veh. Technol.*, vol. 63, no. 2, pp. 580–590, Feb. 2014.

[11] Z. Sun, J. Zheng, Z. Man, and H. Wang, "Robust control of a vehicle Steer-by-Wire system using adaptive sliding mode," *IEEE Trans. Ind. Electron.*, vol. 63, no. 4, pp. 2251–2262, Apr. 2016.

[12] H. Wang, Z. Man, W. Shen, Z. Cao, J. Zheng, J. Jin, and D. M. Tuan, "Robust control for Steer-by-Wire systems with partially known dynamics," *IEEE Trans. Ind. Informat.*, vol. 10, no. 4, pp. 2003–2015, Nov. 2014.

[13] M. Matsuoka, T. Murakami, and K. Ohnishi, "Vibration suppression and disturbance rejection control of a flexible link arm," in *Proc. IECON*, vol. 2, Nov. 1995, pp. 1260–1265.

[14] P. Koronki, H. Hashimoto, and V. Utkin, "Direct torsion control of flexible shaft in an observer-based discrete-time sliding mode," *IEEE Trans. Ind. Electron.*, vol. 45, no. 2, pp. 291–296, Apr. 1998.

[15] Y.-F. Li, B. Eriksson, and J. Wikander, "Sliding mode control of two-mass positioning systems," *IFAC Proc. Volumes*, vol. 32, no. 2, pp. 1166–1171, 1999.

[16] A. Šabanović, K. Jezernik, and K. Wada, "Chattering-free sliding modes in robotic manipulators control," *Robotica*, vol. 14, no. 1, pp. 17–29, 1996.

[17] A. Hace, K. Jezrnik, and A. Sabanović, "SMC with disturbance observer for a linear belt drive," *IEEE Trans. Ind. Electron.*, vol. 54, no. 6, pp. 3402–3412, Dec. 2007.

[18] K. Cho, J. Kim, S. B. Choi, and S. Oh, "A high-precision motion control based on a periodic adaptive disturbance observer in a PMLSM," *IEEE/ASME Trans. Mechatronics*, vol. 20, no. 5, pp. 2158–2171, Oct. 2015.

[19] B. K. Kim and W. K. Chung, "Advanced disturbance observer design for mechanical positioning systems," *IEEE Trans. Ind. Electron.*, vol. 50, no. 6, pp. 1207–1216, Dec. 2003.

[20] Z. Yao, J. Yao, and W. Sun, "Adaptive RISE control of hydraulic systems with multilayer neural-networks," *IEEE Trans. Ind. Electron*, vol. 66, no. 11, pp. 8638–8647, Nov. 2019. doi: 10.1109/TIE.2018.2886773.

[21] H. Y. Jo, U. K. Lee, and M. S. Kam, "Development of the independent-type steer-by-wire system using HILS," *Int. J. Automot. Technol.*, vol. 7, no. 3, pp. 311–317, 2006.

[22] C. Zong, H. Xiang, L. He, and F. Sha, "Study on control method of dual-motor for steer-by-wire system," in *Proc. 2nd Int. Conf. Consum. Electron. Commun. Netw. (CECNet)*, Yichang, China, Apr. 2012, pp. 2890–2893.

[23] B. Zheng, C. Altemare, and S. Anwar, "Fault tolerant steer-by-wire road wheel control system," in *Proc. Amer. Control Conf.*, Jun. 2005, pp. 1619–1624.

[24] K. Sakata and H. Fujimoto, "Master-slave synchronous position control for precision stages based on multirate control and dead-time compensation," in *Proc. IEEE/ASME Int. Conf. Adv. Intell. Mechatronics*, Jul. 2009, pp. 263–268.

[25] K. K. Tan, S. Y. Lim, S. Huang, H. F. Dou, and T. S. Giam, "Coordinated motion control of moving gantry stages for precision applications based on an observer-augmented composite controller," *IEEE Trans. Control Syst. Technol.*, vol. 12, no. 6, pp. 984–991, Nov. 2004.

[26] M. Tomizuka, J.-S. Hu, and T.-C. Chiu, " Synchronization of two motion control axes under adaptive Feedforward control," *ASME J. Dyn. Syst. Meas. Control*, vol. 114, no. 6, pp. 196–203, 1992.

HYEONGJIN HWANG received the B.S. degree in mechanical engineering from Yeungnam University, Gyeongbuk, South Korea, in 2018, where he is currently pursuing the master's degree in mechanical engineering. His research interests include mechatronics system control and precision motion control.

HYUNGJEEN CHOI received the B.S. degree in mechanical engineering and electronics from Dongguk University, South Korea, and the M.S. degree in mechatronics from the Gwangju Institute of Science and Technology, South Korea. He is currently pursuing the Ph.D. degree in mechanical engineering with the Korea Advanced Institute of Science and Technology (KAIST), South Korea.

Since 2004, he has been with Korea Automotive Technology Institute (KATECH). His research interests include vehicle dynamics and control, active control systems, advanced driver assistance systems (ADAS), autonomous vehicle control, and micro-mobility.

KANGHYUN NAM received the B.S. degree in mechanical engineering from Kyungpook National University, Daegu, South Korea, in 2007, the M.S. degree in mechanical engineering from the Korea Advanced Institute of Science and Technology, Daejeon, South Korea, in 2009, and the Ph.D. degree in electrical engineering from The University of Tokyo, Tokyo, Japan, in 2012.

From 2012 to 2015, he was a Senior Engineer with Samsung Electronics Company Ltd., Gyeonggi, South Korea. Since 2015, he has been an Assistant Professor with the School of Mechanical Engineering, Yeungnam University, Gyeongbuk, South Korea. His research interests include vehicle motion control, steer-by-wire system control, and in-wheel-motor-driven electric vehicles.

Prof. Nam is a member of the Korean Society of Automotive Engineers. He was a recipient of the Best Paper Award from the IEEE TRANSACTIONS ON INDUSTRIAL ELECTRONICS, in 2014. He is also an Associate Editor of the IEEE TRANSACTIONS ON VEHICULAR TECHNOLOGY.